

# Spin–Orbit Interaction in Single Wall Carbon Nanotubes: Symmetry Adapted Tight-Binding Calculation and Effective Model Analysis

Wataru IZUMIDA\*, Kentaro SATO, and Riichiro SAITO

*Department of Physics, Tohoku University, Sendai 980-8578*

(Received February 17, 2009; accepted April 27, 2009; published June 25, 2009)

Energy band for single wall carbon nanotubes with spin–orbit interaction is calculated using non-orthogonal tight-binding method. A Bloch function with spin degree of freedom is introduced to adapt the screw symmetry of nanotubes. The energy gap opened by spin–orbit interaction for armchair nanotubes, and the energy band splitting for chiral and zigzag nanotubes are evaluated quantitatively. Spin polarization direction for each split band is shown to be parallel to the nanotube axis. The energy gap and the energy splitting depend on the diameter and chirality in an energy scale of sub-milli-electron volt. An effective model for reproducing the low energy band structure shows that the two mechanism of the band modification, shift of the energy band in two dimensional reciprocal lattice space, and, effective Zeeman energy shift, are relevant. The effective model explains well the energy gap and splitting for more than 300 nanotubes within the diameter between 0.7 to 2.5 nm.

KEYWORDS: carbon nanotube, spin–orbit interaction, screw symmetry, tight-binding calculation  
DOI: [10.1143/JPSJ.78.074707](https://doi.org/10.1143/JPSJ.78.074707)

## 1. Introduction

Carbon nanotubes are new candidates for molecular nanoconductors.<sup>1)</sup> Because of a unique electronic property, being either metallic or semiconducting depending on their cylindrical geometry,<sup>2–7)</sup> nanotubes as charge conductors have been studied extensively. Spin properties, on the other hand, have also been investigated with both scientific and engineering interests. Spin-dependent current injected from ferro-magnetic lead demonstrates that spin scattering length is longer, at least, than the nanotube length which is typically sub-micron.<sup>8–18)</sup> Moreover, spin states in carbon nanotube quantum dot seems to be independent from the orbital as shown the four-electron shell structure.<sup>19–28)</sup> These experiments seem to be consistent with an expectation of few spin scattering events in carbon materials, because of relatively small spin–orbit interaction in a carbon atom.

Since the spin–orbit splitting of a carbon atom has been expected to be a few milli-electron volt,<sup>29–33)</sup> the effect of spin–orbit interaction in carbon nanotubes might appear at low temperatures. In the recent experiment, small energy splitting has been observed by transport measurement, and it is considered that the spin–orbit interaction is relevant to the splitting.<sup>34)</sup> Using the perturbative approach, several groups<sup>30,32)</sup> have shown that an energy gap opens for the energy bands which cross at the Fermi energy, and that the energy bands split for the other energy bands by the spin–orbit interaction. Numerical tight-binding calculation<sup>35)</sup> has shown that the spin–orbit interaction lifts the spin degeneracy of energy bands for chiral nanotubes due to the lack of inversion symmetry, while the spin degeneracy survives for achiral nanotubes. However, an unrealistic large spin–orbit coupling parameter has been assumed in the calculation.<sup>35)</sup> The previous theories<sup>30,32,35,36)</sup> can not explain the experimental behaviors, such as asymmetric splitting between conduction and valence bands<sup>34)</sup> and chirality dependence of spin–orbit interaction. In this paper, quantitative and system-

atic calculation of single-particle spectrum including the spin–orbit interaction for a variety of nanotubes is presented to understand the low energy excitations in carbon nanotubes.

Screw symmetry of single wall carbon nanotubes enables to map the nanotube problem to that of the two-dimensional graphene.<sup>37)</sup> In this paper, we adopt the screw symmetry in the non-orthogonal tight-binding model<sup>38,39)</sup> using 2s and 2p electrons of carbon atom, to calculate the electronic properties of carbon nanotubes. By taking into account the cylindrical structure of nanotubes, optimization of the structure, and by using a density-functional theory framework for transfer and overlap integrals,<sup>40)</sup> quantitative calculation for all types of spinless nanotubes has been well established.<sup>38,39)</sup> In the screw symmetry-adapted framework,  $2p_x$ ,  $2p_y$ , and  $2p_z$  atomic orbitals of tight-binding Bloch function are defined on the curved surface coordinates of nanotubes.

For the spin problem with spin–orbit interaction, product of a spinless Bloch function and a spin function is generally adopted for the basis set for the Hamiltonian, which is utilized in the perturbative approach.<sup>30,32,36)</sup> However, the product can not be used for the symmetry-adapted Bloch function. It is because that the orbitals in an atom is defined for each coordinate axis of the atom while the axes for the spin does not change. Thus only the one-dimensional periodicity of nanotubes can be used in the numerical tight-binding calculation<sup>35)</sup> in which the spin function is defined in the three-dimensional coordinates, which requires a large matrix size for the calculation.

In this paper we introduce a symmetry adapted Bloch function with spin degree of freedom. This Bloch function allows us to reduce the matrix size up to  $16 \times 16$  (2 atoms  $\times$  4 orbitals (2s,  $2p_x$ ,  $2p_y$ ,  $2p_z$  orbitals)  $\times$  2 spin degree of freedom) for any nanotubes. Then we calculate the energy band structure numerically for about 300 single wall carbon nanotubes whose diameter from 0.7 to 2.5 nm. We will show that the spin–orbit interaction induces a small energy gap at the Fermi energy for armchair nanotubes, which does not have any curvature induced energy gap.<sup>3,4,30,41)</sup> For chiral and zigzag nanotubes, the spin-

\*E-mail: izumida@cmt.phys.tohoku.ac.jp

degenerate energy bands split into two due to the spin-orbit interaction. The spin polarization direction for each band is parallel to the nanotube axis. The splitting shows diameter and chirality dependences, and is generally asymmetric between conduction and valence bands. An effective model for spin-orbit interaction is also derived using second order perturbation theory at  $K$  and  $K'$  points. Two mechanism, (i) shift of the energy band in two dimensional reciprocal lattice space, which has been pointed out in the previous studies,<sup>30,32,36</sup> and (ii) effective Zeeman term given in the present paper, are relevant. Together with the curvature induced spin-independent term,<sup>30</sup> the diameter and chirality dependences of energy band are understood qualitatively by the effective model.

This paper is organized as follows. In §2, a Bloch condition and tight-binding function are given to calculate the spin-orbit interaction for tubular materials. In §3, the energy band calculations for armchair, chiral and zigzag nanotubes are shown. The diameter dependence of the energy gap for armchair nanotubes and the fitted function of the gap are also given. In §4, the diameter and chirality dependences of energy splitting are shown for chiral and zigzag nanotubes in diameter 0.7 to 2.5 nm. In §5, an effective model is introduced to explain the origin of the diameter and chirality dependences. In §6, comparison with the experiment and the other theories is given. In §7, the conclusion of this paper is given.

## 2. Formulation

A single wall carbon nanotube is defined by a rolled-up graphene sheet. For the graphene, two carbon atoms in an unit cell, A and B atoms, can be mapped onto the entire graphene sheet by the two unit vectors,  $\mathbf{a}_1$  and  $\mathbf{a}_2$ .<sup>42</sup> Structure of a single wall carbon nanotube is determined by two integers,  $(n, m)$ , which define the chiral vector,  $\mathbf{C}_h = n\mathbf{a}_1 + m\mathbf{a}_2$ , in two-dimensional graphene sheet. The unit vector of nanotube is then defined by the translation vector  $\mathbf{T} = t_1\mathbf{a}_1 + t_2\mathbf{a}_2$ , where  $t_1 = (2m + n)/d_R$ ,  $t_2 = -(2n + m)/d_R$ ,  $d_R$  is the greatest common divisor of  $2n + m$  and  $2m + n$ . The one-dimensional nanotube unit cell contains  $2N = 4(n^2 + nm + m^2)/d_R$  carbon atoms, which are much larger than two, especially for chiral nanotubes. This means that a large matrix size is needed for the electronic state calculation when we consider only one-dimensional periodicity.

When we adopt the screw symmetry, the unit cell consists of only two carbon atoms. Here let us consider a nanotube in the  $XYZ$ -coordinate system, where the nanotube axis coincides with the  $Z$  axis as shown in Fig. 1. The A (or B) atom can be mapped onto the entire tube by two screw operations,  $\mathcal{S}_u$  ( $u = 1, 2$ ), which corresponds to the operation with  $\mathbf{a}_u$  on two-dimensional graphene sheet. The two screw operations are defined as the product of two operations,

$$\mathcal{S}_u = \mathcal{T}(T_u)\mathcal{R}(\Theta_u), \quad (u = 1, 2), \quad (2.1)$$

where  $\mathcal{T}(T_u)$  is the translation operator of  $T_u$  in the axis direction,  $\mathcal{R}(\Theta_u)$  is the rotation operator of angle  $\Theta_u$  in the circumference direction (see Fig. 1). The components of two screw operations satisfy the relations,  $n\Theta_1 + m\Theta_2 = 2\pi$ ,  $nT_1 + mT_2 = 0$  for the circumference direction,  $t_1\Theta_1 + t_2\Theta_2 = 0$ ,  $t_1T_1 + t_2T_2 = T$  for the axis direction, respective-

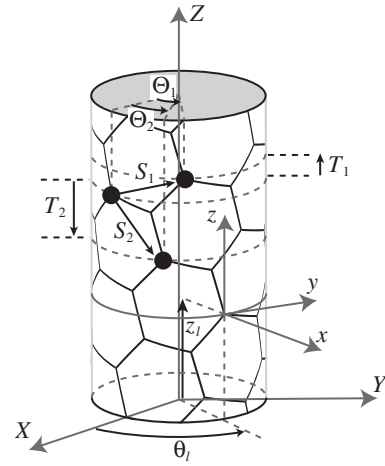


Fig. 1. Two screw operations  $\mathcal{S}_u$  ( $u = 1, 2$ ), and the  $XYZ$ - and  $xyz$ -coordinates. All carbon atoms are on the cylindrical surface.  $\mathcal{S}_u$  is the product of operations with axis and circumference components  $T_u$  and  $\Theta_u$ , respectively. Surface coordinates are denoted by  $(x, y, z)$  which are defined at each atomic position at  $(r \cos \theta_l, r \sin \theta_l, z_l)$ . The  $x$  axis is chosen in the direction normal to the cylinder surface, the  $y$  axis in the circumference direction, and the  $z$  axis in the nanotube axis direction. Three-dimensional coordinates are denoted by  $(X, Y, Z)$ .

ly. Here  $T = \sqrt{3}\pi d_t/d_R$  is the length of nanotube unit cell,  $d_t$  is the diameter of nanotube.

The spinless, screw-symmetry-adapted, tight-binding Bloch function is defined as follows,<sup>37-39</sup>

$$|j\sigma\mathbf{k}\rangle = \frac{1}{\sqrt{N_s}} \sum_l e^{ikz_l + i\mu\theta_l} |\phi_{j\sigma l}\rangle, \quad (2.2)$$

where  $j = 2s$ ,  $x$ ,  $y$ ,  $z$  is the index for  $2s$ ,  $2p_x$ ,  $2p_y$ ,  $2p_z$  orbitals, respectively,  $\sigma = 1$  ( $-1$ ) denotes A (B) atom in the two-atom unit cell.  $\mathbf{k} = (k, \mu)$  is an one-dimensional wave-vector with  $-\pi/T \leq k < \pi/T$ , for subband indices  $\mu = 0, \dots, N - 1$  which corresponds to the circumference momentum.  $|\phi_{j\sigma l}\rangle$  is the  $j$ -th atomic orbital at the  $l$ -th atomic site  $\mathbf{r}_l = (r \cos \theta_l, r \sin \theta_l, z_l)$ , with  $r = d_t/2$ , in which  $d_t$  is the diameter of nanotube. The summation on  $l$  in eq. (2.2) is taken over the  $N_s$   $\sigma$ -atoms, in which  $N_s$  is the number of the two-atom unit cell. The direction of the atomic orbitals is defined at each atom with the  $xyz$ -coordinate system (see Fig. 1), in which the  $x$  axis is chosen in the direction normal to the cylinder surface, the  $y$  axis in the circumference direction, and the  $z$  axis in the nanotube axis direction. Thus, the  $\pi$  band consists of mainly from  $p_x$ -orbitals (not  $p_z$  in the conventional notation) in our coordinates. The atomic orbital satisfies the relation,  $\mathcal{T}(z_l)\mathcal{R}(\theta_l)|\phi_{j\sigma l=0}\rangle = |\phi_{j\sigma l}\rangle$ , where the label  $l = 0$  indicates the atom at the origin  $(X, Y, Z) = (r, 0, 0)$ . The function in eq. (2.2) satisfies the Bloch condition,

$$\mathcal{S}_u |j\sigma\mathbf{k}\rangle = e^{-ikT_u - i\mu\Theta_u} |j\sigma\mathbf{k}\rangle. \quad (2.3)$$

The spin-independent Hamiltonian is given by,

$$H_0 = \frac{\mathbf{p}^2}{2m_e} + V(\mathbf{r}), \quad (2.4)$$

where  $\mathbf{p}$  is the momentum operator,  $m_e$  is the mass of an electron,  $V(\mathbf{r})$  is the crystal potential. The  $8 \times 8$  Hamiltonian matrix elements and the overlap integral between the Bloch functions defined by eq. (2.2) are written as,

$$\begin{aligned} \langle j\sigma\mathbf{k}|H_0|j'\sigma'\mathbf{k}'\rangle &= \sum_l' e^{-ikz_l - i\mu\theta_l} \langle \phi_{j\sigma l}|H_0|\phi_{j'\sigma' l=0}\rangle \delta_{\mathbf{k},\mathbf{k}'} \\ &\equiv H_{0,j\sigma,j'\sigma'}^{\text{sl}} \delta_{\mathbf{k},\mathbf{k}'}, \end{aligned} \quad (2.5)$$

$$\begin{aligned} \langle j\sigma\mathbf{k}|j'\sigma'\mathbf{k}'\rangle &= \sum_l' e^{-ikz_l - i\mu\theta_l} \langle \phi_{j\sigma l}|\phi_{j'\sigma' l=0}\rangle \delta_{\mathbf{k},\mathbf{k}'} \\ &\equiv S_{j\sigma,j'\sigma'}^{\text{sl}} \delta_{\mathbf{k},\mathbf{k}'}. \end{aligned} \quad (2.6)$$

The matrix elements between atomic orbitals,  $\langle \phi_{j\sigma l}|H_0|\phi_{j'\sigma' l=0}\rangle$  and  $\langle \phi_{j\sigma l}|\phi_{j'\sigma' l=0}\rangle$ , have been evaluated by the *ab initio* calculation.<sup>40)</sup> By solving the secular equation,  $[H_0^{\text{sl}} - E_0^{\text{sl}} S^{\text{sl}}] \mathbf{C}^{\text{sl}} = 0$ , 8 eigenvalues  $E_0^{\text{sl}}(\mathbf{k})$  and 8 eigenvectors  $\mathbf{C}^{\text{sl}}$  are given.

Let us consider the spin-orbit interaction as an additional term to  $H_0$ . Relevant contribution of the spin-orbit interaction comes from each atomic site. Under the atomic potential in each site, the spin-orbit interaction of the system can be expressed by,

$$H_{\text{so}} = \frac{1}{2} V_{\text{so}} \sum_l \boldsymbol{\ell}_l \cdot \mathbf{s}. \quad (2.7)$$

Here  $\boldsymbol{\ell}_l$  is the angular momentum operator acts on the atomic orbitals at site  $l$ ,  $\mathbf{s}$  is the Pauli spin matrix, and  $V_{\text{so}}$  is the spin-orbit coupling constant. The summation on  $l$  in eq. (2.7) is taken over the  $2N_s$  atoms. In this paper we consider only the on-site spin-orbit interaction.

If we define the product of the spinless Bloch function and a spin function,

$$|j\sigma\mathbf{s}\mathbf{k}\rangle = |j\sigma\mathbf{k}\rangle|s\rangle = \frac{1}{\sqrt{N_s}} \sum_l' e^{ikz_l + i\mu\theta_l} |\phi_{j\sigma l}\rangle|s\rangle, \quad (2.8)$$

it is clear that eq. (2.8) does not satisfy the Bloch condition, that is,  $\mathcal{S}_u|j\sigma\mathbf{s}\mathbf{k}\rangle \neq c|j\sigma\mathbf{s}\mathbf{k}\rangle$ , where  $c$  is a constant factor, and  $|s\rangle$  is an eigenfunction of  $\mathbf{s} \cdot \mathbf{n}_\alpha$ ,  $\mathbf{n}_\alpha$  is a unit vector of  $\alpha$ -direction in the XYZ coordinate system. Hereafter, let  $\alpha = Z$ , that is,  $|s\rangle$  is the eigenfunction of  $s_Z$ , where  $s_Z$  is the Z component of the Pauli matrix.  $s = 1$  ( $-1$ ) is the spin index for up (down) state. Even for this choice of the spin function, eq. (2.8) is not suitable as a symmetry adapted Bloch function for the presence of spin-orbit interaction. In fact, the matrix elements of spin-orbit interaction between the functions of eq. (2.8),  $\langle x\sigma\mathbf{s}\mathbf{k}|H_{\text{so}}|z\sigma - \mathbf{s}\mathbf{k}'\rangle = (1/2)sV_{\text{so}}\delta_{\mathbf{k},\mathbf{k}'}\delta_{\mu,\mu'-s}$ , have the non-zero matrix elements between different wave numbers [see Appendix eq. (A.27)], because of the azimuth-angle dependent factor on  $\langle s|\langle \phi_{x\sigma l}|H_{\text{so}}|\phi_{z\sigma l}\rangle|-s\rangle = (1/2)e^{-i\theta_l s} sV_{\text{so}}$  reflecting that the coordinate system for atomic orbital is rotated by  $\theta_l$  from the fixed coordinate system for the spin function.

In order to avoid this problem, we define the symmetry adapted tight-binding Bloch function as a linear combination of the orbital,  $|\phi_{j\sigma l}\rangle|s_l\rangle$ , with the same Bloch phase for the opposite spin states. The state  $|s_l\rangle$  is a spin-1/2 eigenfunction defined in the surface coordinates at  $l$ , and its quantization axis should be the same for all  $l$  in the sense of the surface coordinates. In the present problem we use the following function as  $|s_l\rangle$ ,

$$|s_l\rangle = \mathcal{R}(\theta_l)|s\rangle = \exp\left(-i\frac{s\theta_l}{2}\right)|s\rangle. \quad (2.9)$$

Note that  $\mathcal{T}(z_l)$  operation doesn't affect the spin function. Hereafter we use the following tight-binding function,

$$|j\sigma\tilde{\mathbf{s}}\mathbf{k}_J\rangle = \frac{1}{\sqrt{N_s}} \sum_l' e^{ikz_l + iJ\theta_l} |\phi_{j\sigma l}\rangle|s_l\rangle, \quad (2.10)$$

where  $\mathbf{k}_J = (\mathbf{k}, J)$ ,  $J = \mu_J + 1/2$  is a half-integer,  $\mu_J = 0, \dots, N-1$  are subband indices for the presence of spin-orbit interaction. The symbol tilde on spin index  $s$  is put to emphasize that the spin state of Bloch function is different from that defined in the XYZ-coordinates, but is the linear combination of spin states which are defined on the surface coordinates at each atomic site. In the sense of angular momentum,  $J$  corresponds to total angular momentum for spin up with  $\mu$  and spin down with  $\mu + 1$  states. For the presence of spin-orbit interaction,  $\mu$  is not a good quantum number. Therefore the index  $\mu_J$  is convenient to use for the subband index in the present problem. The function (2.10) now satisfies the following Bloch condition,

$$\mathcal{S}_u|j\sigma\tilde{\mathbf{s}}\mathbf{k}_J\rangle = e^{-ikT_u - iJ\Theta_u}|j\sigma\tilde{\mathbf{s}}\mathbf{k}_J\rangle. \quad (2.11)$$

The Bloch condition eq. (2.11) has two phase factors which come from the rotational boundary and translational periodic boundary conditions. The rotational boundary condition is written as,  $\mathcal{R}(2\pi)|j\sigma\tilde{\mathbf{s}}\mathbf{k}_J\rangle = -|j\sigma\tilde{\mathbf{s}}\mathbf{k}_J\rangle$ , where the minus sign reflects that the spin function changes its sign under the  $2\pi$  rotation. Therefore, the additional factor  $\exp(-i\Theta_u/2)$  appears in eq. (2.11) from the spinless case of eq. (2.3).

For  $H_{\text{so}}$ , we have non-zero atomic matrix elements as follows,

$$\langle s_l|\langle \phi_{x\sigma l}|H_{\text{so}}|\phi_{y\sigma l}\rangle|s_l\rangle = -\frac{i}{2}s_lV_{\text{so}}, \quad (2.12)$$

$$\langle s_l|\langle \phi_{x\sigma l}|H_{\text{so}}|\phi_{z\sigma l}\rangle|-s_l\rangle = \frac{1}{2}s_lV_{\text{so}}, \quad (2.13)$$

$$\langle s_l|\langle \phi_{y\sigma l}|H_{\text{so}}|\phi_{z\sigma l}\rangle|-s_l\rangle = -\frac{i}{2}V_{\text{so}}. \quad (2.14)$$

Here we note that the matrix elements have no azimuth-angle dependence. Then the corresponding matrix elements between the Bloch functions of eq. (2.10) are written as,

$$\begin{aligned} \langle x\sigma\tilde{\mathbf{s}}\mathbf{k}_J|H_{\text{so}}|y\sigma\tilde{\mathbf{s}}\mathbf{k}'_J\rangle &= -\frac{i}{2}\tilde{s}V_{\text{so}}\delta_{\mathbf{k}_J,\mathbf{k}'_J} \\ &\equiv H_{\text{so},x\sigma\tilde{s},y\sigma\tilde{s}}\delta_{\mathbf{k}_J,\mathbf{k}'_J}, \end{aligned} \quad (2.15)$$

$$\begin{aligned} \langle x\sigma\tilde{\mathbf{s}}\mathbf{k}_J|H_{\text{so}}|z\sigma - \tilde{\mathbf{s}}\mathbf{k}'_J\rangle &= \frac{1}{2}\tilde{s}V_{\text{so}}\delta_{\mathbf{k}_J,\mathbf{k}'_J} \\ &\equiv H_{\text{so},x\sigma\tilde{s},z\sigma - \tilde{s}}\delta_{\mathbf{k}_J,\mathbf{k}'_J}, \end{aligned} \quad (2.16)$$

$$\begin{aligned} \langle y\sigma\tilde{\mathbf{s}}\mathbf{k}_J|H_{\text{so}}|z\sigma - \tilde{\mathbf{s}}\mathbf{k}'_J\rangle &= -\frac{i}{2}V_{\text{so}}\delta_{\mathbf{k}_J,\mathbf{k}'_J} \\ &\equiv H_{\text{so},y\sigma\tilde{s},z\sigma - \tilde{s}}\delta_{\mathbf{k}_J,\mathbf{k}'_J}. \end{aligned} \quad (2.17)$$

Matrix elements of spin-independent Hamiltonian  $H_0$  and overlap integral between the Bloch function (2.10) are written as,

$$\begin{aligned} \langle j\sigma\tilde{\mathbf{s}}\mathbf{k}_J|H_0|j'\sigma'\tilde{\mathbf{s}}\mathbf{k}'_J\rangle &= \sum_l' \exp(-ikz_l - i\mu_J\theta_l) \\ &\quad \times \exp\left(-i\frac{1-\tilde{s}}{2}\theta_l\right) \langle \phi_{j\sigma l}|H_0|\phi_{j'\sigma' l=0}\rangle \delta_{\mathbf{k}_J,\mathbf{k}'_J} \\ &\equiv H_{0,j\sigma\tilde{s},j'\sigma'\tilde{s}}\delta_{\mathbf{k}_J,\mathbf{k}'_J}, \end{aligned} \quad (2.18)$$

$$\begin{aligned}
 & \langle j\sigma\tilde{s}k_J | j'\sigma'\tilde{s}'k'_J \rangle \\
 &= \sum_l \exp(-ikz_l - i\mu_J\theta_l) \\
 & \times \exp\left(-i\frac{1-\tilde{s}}{2}\theta_l\right) \langle \phi_{j\sigma l} | \phi_{j'\sigma' l=0} \rangle \delta_{k_J, k'_J} \\
 & \equiv S_{j\sigma\tilde{s}, j'\sigma'\tilde{s}'} \delta_{k_J, k'_J}.
 \end{aligned} \tag{2.19}$$

Even though the Hamiltonian  $H_0$  itself doesn't contain a spin-dependent term, the spin dependent factor  $\exp\{-i[(1-\tilde{s})/2]\theta_l\}$  appears in the matrix element in eq. (2.18) [also in eq. (2.19)] because of the Bloch function (2.10). Therefore we have the same matrix elements between spin "down" state ( $\tilde{s} = -1$ ) of  $(\mu_J - 1)$ -th subband and spin "up" state ( $\tilde{s} = 1$ ) of  $\mu_J$ -th subband as follows,

$$H_{0, j\sigma\tilde{s}=-1, j'\sigma'\tilde{s}'=1}(k, \mu_J - 1) = H_{0, j\sigma\tilde{s}=1, j'\sigma'\tilde{s}'=1}(k, \mu_J). \tag{2.20}$$

Thus it is important to note that for the absence of spin-orbit interaction,  $V_{so} = 0$ , the two-fold spin degeneracy occurs between the  $\mu_J$ -th and  $(\mu_J - 1)$ -th energy subbands,

$$E_{0, \tilde{s}=-1}(k, \mu_J - 1) = E_{0, \tilde{s}=1}(k, \mu_J), \tag{2.21}$$

which is independent of the degeneracy of energy bands due to the time-reversal and inversion symmetries.<sup>35)</sup> When we use eq. (2.8) for the basis sets of Hamiltonian matrix, for  $V_{so} = 0$ , the two-fold spin degeneracy occurs in the same subband,  $E_{0, \tilde{s}=-1}(k, \mu) = E_{0, \tilde{s}=1}(k, \mu)$ .

In the presence of spin-orbit interaction, eigenvalues  $E_\lambda(\mathbf{k}_J)$  and eigenvectors  $\mathbf{C}_\lambda$  ( $\lambda = 1, \dots, \Lambda$ ) are given by solving the secular equation,  $[H - E_\lambda S]\mathbf{C}_\lambda = 0$ , in which,  $H_{j\sigma\tilde{s}, j'\sigma'\tilde{s}'} = H_{0, j\sigma\tilde{s}, j'\sigma'\tilde{s}'} + H_{so, j\sigma\tilde{s}, j'\sigma'\tilde{s}'}$  is the matrix element of the total Hamiltonian,  $\Lambda = \sum_j \sum_\sigma \sum_{\tilde{s}} = 16$ . As shown in eqs. (2.15) and (2.16), since  $p_x$ -orbital, which is relevant to  $\pi$  band, has the matrix elements between  $p_y$  and  $p_z$ -orbitals ( $\sigma$  band), the spin-orbit interaction induces the  $\sigma$ - $\pi$  hybridization. It is well known that the curvature of nanotube induces the  $\sigma$ - $\pi$  hybridization,<sup>3,4,30,41)</sup> too. We will show how these two effects appear in energy band structure.

### 3. Energy Band for Achiral and Chiral Nanotubes

We calculate energy band for achiral and chiral nanotubes by solving the secular equation. The atomic hopping and overlap integrals,  $\langle \phi_{j\sigma l} | H_0 | \phi_{j'\sigma' l=0} \rangle$  and  $\langle \phi_{j\sigma l} | \phi_{j'\sigma' l=0} \rangle$ , in eqs. (2.18) and (2.19) are taken into account up to 10 bohr  $\sim 5 \text{ \AA}$  distance. These integrals are estimated from the *ab initio* calculation.<sup>40)</sup> The curvature induced hybridization is automatically taken into account. Optimization of the structure<sup>38)</sup> has also performed so as to minimize the total energy with inter-atomic potential which is also given by the *ab initio* calculation.<sup>40)</sup>

In Fig. 2, the energy band of  $(n, m) = (6, 6)$  armchair nanotube is shown. Because the low energy properties are the main interest in this paper, only energy region near the Fermi level is shown. In the calculation, spin-orbit coupling constant  $V_{so} = 6 \text{ meV}$  is used, which is estimated by the local spin density calculation for an isolated carbon atom.<sup>31,43)</sup> Because  $V_{so}$  for the nanotube might be different than that of an isolated atom, calculations for other  $V_{so}$  values have also been done, as shown later. For comparison, energy band without spin-orbit interaction is also shown as the dashed line in the inset of Fig. 2. For the absence of spin-orbit interaction, the two linear bands cross at the Fermi energy

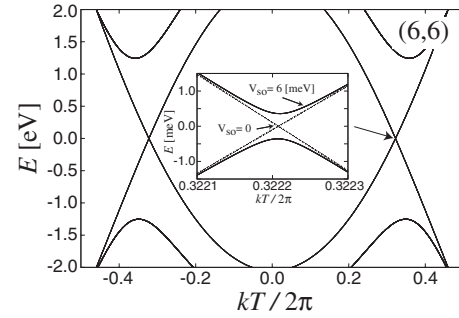


Fig. 2. Energy band of (6,6) armchair nanotube. Spin-orbit coupling constant is  $V_{so} = 6 \text{ meV}$ . Inset shows in larger scale near the Fermi energy. The dashed line in the inset is the energy band calculation for the absence of spin-orbit interaction.

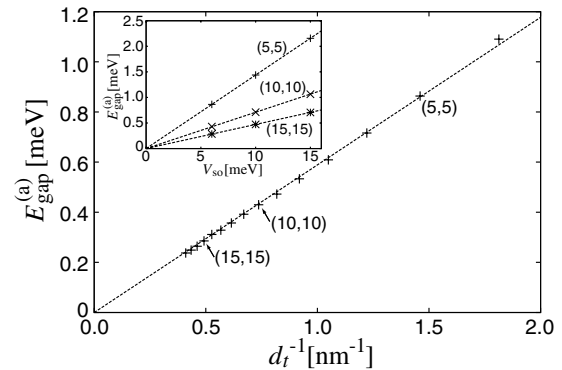


Fig. 3. Energy gap of armchair nanotubes, as a function of inverse of nanotube diameter. Spin-orbit coupling constant is  $V_{so} = 6 \text{ meV}$ . Inset: Energy gap of armchair nanotubes, as a function of spin-orbit coupling constant.

near  $kT = 2\pi/3$  ( $-2\pi/3$ ). Note that the crossing points are shifted to the smaller  $|k|$ ,  $kT/2\pi \simeq \pm(1/3 - 0.0111)$ , because of the curvature effect.<sup>3,30)</sup> It has been pointed out that the armchair nanotubes with small diameter still have the linear band at the Fermi energy, even the other types of chiral and zigzag metallic nanotubes have a small energy gap at the Fermi energy by the curvature effect.<sup>3,4,30,41)</sup> However, the robustness of the metallic nature for armchair nanotubes is broken by the spin-orbit interaction.<sup>30,32,35)</sup> The present calculation shows a small gap ( $\simeq 0.72 \text{ meV}$ ) at the Fermi energy. However, each energy subband still has the two-fold degeneracy, because the spin-orbit interaction does not break the time-reversal symmetry, and the armchair nanotubes have the inversion symmetry.<sup>35)</sup> These properties are consistent with the previous theories.<sup>30,32,35)</sup> The energy gap can be understood as the shift of energy crossing point in two-dimensional  $\mathbf{k}$ -space,<sup>30,32)</sup> as also discussed later.

In Fig. 3, energy gap for armchair nanotubes is plotted as a function of inverse of diameter. The gap as a function of spin-orbit coupling constant  $V_{so}$  is also shown in the inset, because  $V_{so}$  might be different than that of an isolated carbon atom. It is shown that the energy gap is proportional to the inverse of diameter, and to the spin-orbit coupling constant. From the calculation, the energy gap for the armchair nanotubes is estimated as

$$E_{\text{gap}}^{(a)} = a^{(a)} \frac{V_{so}}{d_t}, \tag{3.1}$$

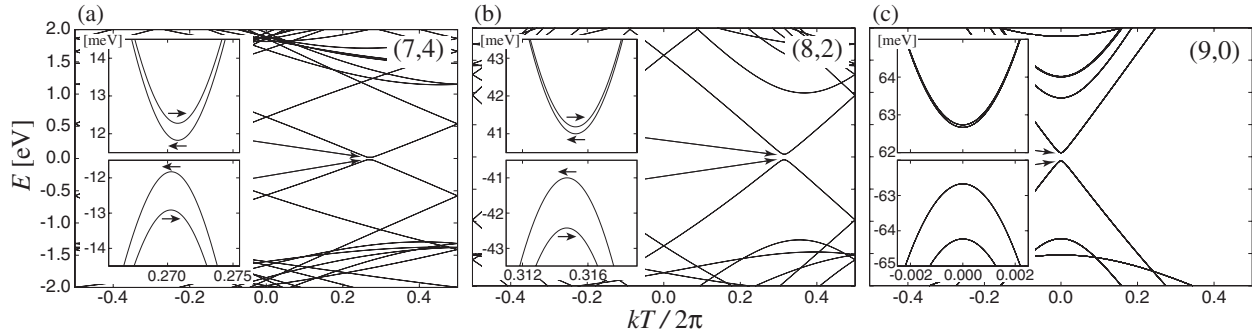


Fig. 4. Energy band of (a) (7, 4), (b) (8, 2), and (c) (9, 0) nanotubes. Spin-orbit coupling constant is  $V_{so} = 6$  meV. Each inset shows in larger scale near the Fermi energy. The arrows indicated on each band in inset show the spin polarization direction, right (left) direction corresponds to the polarization to  $z$  ( $-z$ ) direction.

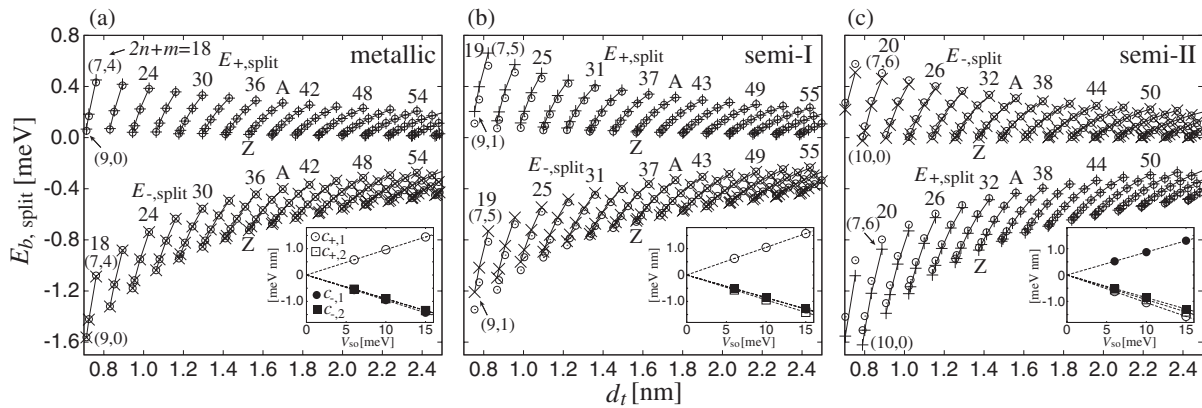


Fig. 5. Energy band splitting as a function of diameter for (a) metallic, (b) type-I semiconducting, (c) type-II semiconducting nanotubes. Spin-orbit coupling constant is  $V_{so} = 6$  meV. The splitting for valence band is shown with symbol  $\times$ , that for conduction band is shown with symbol  $+$ . The numbers indicated on each line are the corresponding  $2n + m$  values. Z (A) denotes  $(n, m)$  value close to zigzag (armchair) nanotube. The fitting function eq. (4.1) for each  $(n, m)$  is also plotted as the open circles. Each inset shows the fitted coefficients,  $c_{b,1/2}^{(v)}$ , in eq. (4.1), as a function of spin-orbit coupling constant  $V_{so}$ .

where the constant is estimated to be  $a^{(a)} = 0.098$  nm. The energy gap expression for the armchair nanotubes, eq. (3.1), will be analytically derived in §5, as a combined effect of the curvature induced  $\sigma$ - $\pi$  hybridization and the spin-orbit interaction.<sup>30,32)</sup>

Figure 4 shows the energy band calculation of (7, 4), (8, 2) chiral, and (9, 0) zigzag nanotubes. The nanotubes of (6, 6), (7, 4), (8, 2), and (9, 0) belong in the same  $2n + m = 18$  metallic family, in which the diameters of nanotubes are similar to one another. First let us discuss on the chiral nanotubes. For the both cases, energy gap opens near the Fermi energy. The energy gap can be understood by the spin-independent curvature effect.<sup>3,4,30,41)</sup> The effect of the spin-orbit interaction appears as the splitting of the energy bands<sup>35)</sup> as shown in the inset of Fig. 4. The arrows indicated on each energy band in the inset show the spin polarization direction to the nanotube axis for each band, where right (left) arrow corresponds to positive (negative) polarization. The calculated result shows that the spin in each energy band is almost perfectly polarized ( $>99\%$ ) to the nanotube axis direction for all  $k$  values shown in inset, and the direction is opposite to each other for the split pair of the energy bands. The splitting of the conduction band [0.45 meV for (7, 4) nanotube, 0.18 meV for (8, 2) nanotube] is smaller than that of the valence band [1.1 meV for (7, 4) nanotube, 1.4 meV for (8, 2) nanotube]. It is a common feature of spin-orbit

splitting in metallic nanotubes. (More quantitative discussion on the splitting will be given in the next section.) Here we note that the energy band at  $-k$  is the same with that at  $k$ , even the spin polarization direction is opposite to each other. For (9, 0) zigzag nanotube, the splitting of energy band caused by the spin-orbit interaction is also seen. However, each band still have the two-fold degeneracy.<sup>35)</sup> Since the two-fold degeneracy is due to the contribution from  $K$  and  $K'$  points, the spin polarization direction between degenerate two bands is opposite to each other.

#### 4. Energy Band Splitting of Chiral and Zigzag Nanotubes

As shown in the previous section, the splitting of energy bands shows the asymmetric splitting between valence and conduction bands and the chirality dependence. To investigate the splitting for many nanotubes, energy splitting at the top (bottom) of the highest valence (lowest conduction) band for all nanotubes with diameter between 0.7 to 2.5 nm is shown as a function of diameter in Fig. 5. The energy splitting is defined as  $E_{b,split} = E_{b,\uparrow} - E_{b,\downarrow}$  where  $b = + (-)$  is the index for the conduction (valence) band, and the arrow ( $\uparrow$  or  $\downarrow$ ) indicates the spin polarization direction.  $E_{+, \uparrow/\downarrow}$  ( $E_{-, \uparrow/\downarrow}$ ) is the energy of bottom of conduction (top of valence) band with corresponding spin polarization. There are two energy-gap points in one-dimensional  $k$ , one comes

from the point near the  $K$  point and the other from the  $K'$  point. In this analysis, we select the one-dimensional Brillouin zone near the  $K$  point, by using the analytic formula that gives  $(k, \mu)$  which is closest to  $K$  point for given  $(n, m)$ .<sup>44</sup>

The results are classified into three cases: metallic [ $\text{mod}(2n + m, 3) = 0$ ], type-I semiconducting [ $\text{mod}(2n + m, 3) = 1$ ] and type-II semiconducting [ $\text{mod}(2n + m, 3) = 2$ ] nanotubes are separately shown. It is shown that the absolute value of splitting becomes larger with decreasing diameter. Moreover the chirality dependence for a given  $2n + m = \text{const.}$  family has also been seen. For the metallic and type-I semiconducting nanotubes, the sign of splitting is negative for valence band and positive for conduction band. As the chiral angle becomes larger (closer to the armchair nanotube), the absolute value of splitting becomes smaller (larger) for the valence (conduction) band. (The chiral angle  $\theta$  is defined as the angle between the chiral vector and zigzag direction.<sup>42</sup>) For the type-II case, the opposite behaviors to metallic and type-I cases are seen: positive (negative) splitting for the valence (conduction) band, and the absolute value of splitting becomes larger (smaller) for the valence (conduction) band as the chiral angle becomes larger. For the three cases, it is commonly seen that the asymmetry of the splitting between valence and conduction bands becomes smaller with increasing the chiral angle.

Here we introduce a fitting function for the diameter and chirality dependent energy splitting as,

$$E_{b,\text{split}}^{(v)} = \frac{c_{b,1}^{(v)} + c_{b,2}^{(v)} \cos(3\theta)}{d_t}, \quad (4.1)$$

where an integer  $v$  is introduced, to indicate the metallic ( $v = 0$ ), type-I ( $v = 1$ ) or type-II ( $v = -1$ ) nanotubes. The fitted function for each  $(n, m)$  is also plotted in Fig. 5 The fitted coefficients,  $c_{b,1/2}^{(v)}$ , are shown in the each inset. From the calculation of the several spin-orbit coupling constant  $V_{\text{so}}$ , the coefficients are plotted as a function of  $V_{\text{so}}$  in the inset. The diameter and chiral angle dependences of the energy splitting can be reproduced well within 0.06 meV by eq. (4.1) except for very small diameter ( $d_t < 1.0$  nm) of the semiconducting nanotubes. For the metallic nanotube of  $d_t > 0.8$  nm, or larger diameter semiconducting nanotubes  $d_t > 1.5$  nm, eq. (4.1) reproduces quite well, within  $10^{-2}$  meV. Because the absolute value of the coefficients  $c_{b,1}^{(v)}$  for valence ( $b = -$ ) and conduction ( $b = +$ ) bands are the almost same each other, the asymmetry of the splitting is mainly due to the second term of eq. (4.1). Each coefficients is proportional to  $V_{\text{so}}$  as,

$$c_{b,1}^{(v)} = a_{b,1}^{(v)} V_{\text{so}}, \quad \text{and} \quad c_{b,2}^{(v)} = a_{b,2}^{(v)} V_{\text{so}}. \quad (4.2)$$

$a_{b,1}^{(v)}$  and  $a_{b,2}^{(v)}$  are given from the numerical results shown in Fig. 5, and are summarized in Table I. In order to understand the diameter, chirality and type dependences, we will discuss the energy splitting by an effective model analysis in the next section.

## 5. Effective Model Analysis

To understand the chirality dependent splitting, let us consider an effective Hamiltonian of  $\pi$  electrons near the Fermi energy. To derive the effective model, we consider eq. (2.8) for the basis sets of Hamiltonian matrix, in which

Table I. The parameters in eq. (4.2), given by the data shown in Fig. 5. The unit is nm.

	$a_{-,1}^{(v)}$	$a_{-,2}^{(v)}$	$a_{+,1}^{(v)}$	$a_{+,2}^{(v)}$
Metallic ( $v = 0$ )	-0.095	-0.090	0.096	-0.090
Type-I ( $v = 1$ )	-0.087	-0.085	0.105	-0.094
Type-II ( $v = -1$ )	0.087	-0.086	-0.105	-0.093

the spin function is defined in the XYZ-coordinates. The detailed derivation of the effective model will be given in Appendix.

Perturbation expansion at  $K$  and  $K'$  points has been often used for low energy analysis of nanotubes and graphene.<sup>45</sup> The effective Hamiltonian of  $\pi$  electrons with spin-orbit interaction is given by taking the two types of  $\sigma$ - $\pi$  hybridizations using the perturbation theory. The effective Hamiltonian for our system is written as the sum of three terms,  $H_{\pi}^{\text{eff}} = H_{\pi,0}^{\text{eff}} + H_{\pi,\text{soc}}^{\text{eff}} + H_{\pi,\text{cv}}^{\text{eff}}$ . The first term,  $H_{\pi,0}^{\text{eff}}$ , is the effective Hamiltonian without both the spin-orbit interaction and the curvature induced hybridization, and is written as,

$$H_{\pi,0}^{\text{eff}} = \hbar v_F \begin{pmatrix} 0 & k_c - i\tau k_t \\ k_c + i\tau k_t & 0 \end{pmatrix}, \quad (5.1)$$

where  $\tau = 1$  ( $-1$ ) is the index of  $K$  ( $K'$ ) point. The first and second columns of the matrix correspond to  $\pi$  states of A and B atomic sites ( $\sigma = 1$  and  $-1$ ), respectively.  $v_F$  is the Fermi velocity,  $k_c$  is the wave number in the circumference direction,  $k_t$  is that in the axis direction. Both  $k_c$  and  $k_t$  are measured from  $K$  ( $K'$ ) point. For the nanotubes,  $k_c = 2(\mu' - v\tau/3)/d_t$ , where  $\mu'$  is an integer counted from  $K$  ( $K'$ ) point.<sup>44,46</sup> The term  $H_{\pi,0}^{\text{eff}}$  gives the well-known Dirac-cone energy bands in two-dimensional  $\mathbf{k}$ -space. Then we add the two  $\sigma$ - $\pi$  hybridization effects, the spin-orbit interaction and the curvature of nanotubes,<sup>30,32</sup> to  $H_{\pi,0}^{\text{eff}}$ . These effects on  $\pi$  electrons can be taken into account by second order perturbation framework. After long but simple calculation, the following additional terms are obtained (see the derivation of eqs. (A-41) and (A-42) in Appendix),

$$H_{\pi,\text{soc}}^{\text{eff}} = \hbar v_F \begin{pmatrix} \varepsilon_{\text{soc}}^{(\tau)} s / \hbar v_F & -\Delta k_{\text{soc}} s \\ -\Delta k_{\text{soc}} s & \varepsilon_{\text{soc}}^{(\tau)} s / \hbar v_F \end{pmatrix}, \quad (5.2)$$

$$H_{\pi,\text{cv}}^{\text{eff}} = \hbar v_F \begin{pmatrix} 0 & -(\Delta k_{c,\text{cv}}^{(\tau)} - i\tau \Delta k_{t,\text{cv}}^{(\tau)}) \\ -(\Delta k_{c,\text{cv}}^{(\tau)} + i\tau \Delta k_{t,\text{cv}}^{(\tau)}) & 0 \end{pmatrix}, \quad (5.3)$$

where the terms

$$\hbar v_F \Delta k_{\text{soc}} = \alpha_1 \frac{V_{\text{so}}}{d_t}, \quad (5.4)$$

$$\varepsilon_{\text{soc}}^{(\tau)} = \tau \alpha_2 \frac{V_{\text{so}}}{d_t} \cos 3\theta, \quad (5.5)$$

give spin-dependent energy shift, while the term

$$\hbar v_F \Delta k_{c,\text{cv}}^{(\tau)} = \tau \beta \frac{\cos 3\theta}{d_t^2}, \quad (5.6)$$

gives spin-independent energy shift. The term

$$\Delta k_{t,\text{cv}}^{(\tau)} = \tau \zeta \frac{\sin 3\theta}{d_t^2}, \quad (5.7)$$

gives the  $k_t$ -shift in the nanotube energy band. The parameters,  $\alpha_1$ ,  $\alpha_2$ ,  $\beta$ ,  $\zeta$ , are given analytically in simpler tight-binding model (see Appendix). The value will be given by fitting to the numerical calculation, too as below. The term  $H_{\pi,\text{soc}}^{\text{eff}}$  is the result as first order processes of both the spin-orbit coupling and the curvature induced hybridization, whereas  $H_{\pi,\text{cv}}^{\text{eff}}$  the result as second order processes of the curvature induced hybridization. Although the off-diagonal terms in eqs. (5.2) and (5.3) have also been pointed out in the previous studies,<sup>30,32,36</sup> the diagonal term in eq. (5.2) is derived in this study. Both terms should be considered to reproduce the diameter, chirality dependences, and asymmetry of conduction and valence band splitting, as shown

$$E_{s\tau(\pm)}^{(v)}(k_t, \mu') = \varepsilon_{\text{soc}}^{(\tau)} s \pm \hbar v_F \sqrt{\left[ \frac{2(\mu' - \nu\tau/3)}{d_t} - \Delta k_{\text{c,cv}}^{(\tau)} - \Delta k_{\text{soc}s} \right]^2 + (k_t - \Delta k_{\text{t,cv}}^{(\tau)})^2}. \quad (5.8)$$

The first term  $\varepsilon_{\text{soc}}^{(\tau)} s$  in eq. (5.8) results from the diagonal term in eq. (5.2). This term causes the chirality dependent spin splitting, and also the asymmetric splitting between conduction and valence bands together with the terms of the shift of energy crossing point in  $k$ -space,  $\Delta k_{\text{c,cv}}^{(\tau)}$  and  $\Delta k_{\text{soc}s}$ . If the first term is missed,<sup>30,32,36</sup> the splitting between the conduction and valence bands are the same. Comparing with eqs. (4.1) and (4.2), we get the following relation,

$$a_{b,1}^{(v)} = 2b\alpha_1, \quad (\text{for } \nu = 0, 1), \quad (5.9)$$

$$a_{b,1}^{(v)} = -2b\alpha_1, \quad (\text{for } \nu = -1), \quad (5.10)$$

$$a_{b,2}^{(v)} = 2\alpha_2, \quad (\text{for } \nu = 0, \pm 1). \quad (5.11)$$

As shown in eqs. (5.9) and (5.10), the coefficient  $a_{b,1}$  for type-II semiconducting nanotubes has the opposite sign to the metallic and type-I cases. This is because that the nearest cutting line to the energy crossing point for type-II sits on the opposite side to the metallic and type-I. Note that the energy crossing point in two dimensional  $k$ -space is shifted to  $k_c > 0$  ( $k_c < 0$ ) from  $K$  ( $K'$ ) point, by the term of eq. (5.6). Equations (5.9)–(5.11) indicate that the (absolute value of) coefficients for the valence and conduction bands are the same,  $|a_{+,1}^{(v)}| = |a_{-,1}^{(v)}|$ ,  $a_{+,2}^{(v)} = a_{-,2}^{(v)}$ . Indeed, for the metallic nanotubes, the evaluated coefficients shown in Table I reproduce the above relations. However, for the type-I and type-II cases, there are small differences,  $|a_{+,1}^{(v)}| > |a_{-,1}^{(v)}|$ ,  $a_{+,2}^{(v)} < a_{-,2}^{(v)}$ . Moreover, the coefficients have the small type dependence,  $|a_{-,1}^{(\pm 1)}| < |a_{-,1}^{(0)}|$ ,  $|a_{+,1}^{(0)}| < |a_{+,1}^{(\pm 1)}|$ ,  $a_{-,2}^{(0)} < a_{-,2}^{(\pm 1)}$ , and  $a_{+,2}^{(0)} < a_{+,2}^{(\pm 1)}$ . The small deviation from eqs. (5.9)–(5.11) for the semiconductor nanotubes reflects that the energy band deviation from the linear band is relatively large for larger  $\sqrt{k_c^2 + k_t^2}$ . Thus within the effective model of linear band approximation, the parameters,  $\alpha_1$ ,  $\alpha_2$ ,  $\beta$ ,  $\zeta$ , are determined by fitting from the numerical results of the metallic nanotubes. We get  $\alpha_1 = 0.048$  nm and  $\alpha_2 = -0.045$  nm. We also get  $\beta = 24$  meV·nm<sup>2</sup> and  $\zeta = -0.18$  nm from our numerical results of spin-independent energy gap and  $k_t$ -shift for metallic nanotubes.

For the armchair nanotubes, we get the energy gap expression eq. (3.1) from the effective model with,

$$a^{(a)} = 2|\alpha_1|. \quad (5.12)$$

below. The second order contribution of spin-orbit interaction is the order of  $\mu\text{eV}$  and thus can be neglected. In the presented effective model, the spin index  $s$ , denotes two spin states parallel to the nanotube axis, is a good quantum number. However, there are also spin-flip processes between the  $\mu$  and  $\mu \pm 1$  energy subbands in the same order of the perturbation with eq. (5.2). [The explicit expression is given in eq. (A·53) in Appendix.] However, the spin-flip between neighbor subbands can also be neglected in the energy band calculation, because the energy difference between the subbands is sufficiently large.

By diagonalizing the effective Hamiltonian,  $H_{\pi}^{\text{eff}} = H_{\pi,0}^{\text{eff}} + H_{\pi,\text{soc}}^{\text{eff}} + H_{\pi,\text{cv}}^{\text{eff}}$ , we get the energy band expression as

The value  $a^{(a)} = 0.098$  nm estimated in §3 is consistent with eq. (5.12) with  $\alpha_1 = 0.048$  nm estimated from the splitting data of chiral and zigzag nanotubes.

## 6. Discussion

In the previous section, we have introduced the effective Hamiltonian for the  $\pi$  electrons. The Hamiltonian is constituted by three terms, unperturbed term  $H_{\pi,0}^{\text{eff}}$ , the spin-orbit term on curved nanotube surface  $H_{\text{soc}}^{\text{eff}}$  which is proportional to  $V_{\text{so}} d_t^{-1}$ , and the term of spin-independent curvature effect  $H_{\pi,\text{cv}}^{\text{eff}}$  which is proportional to  $d_t^{-2}$ . Even the effect of spin-orbit interaction itself appears only in the term  $H_{\pi,\text{soc}}^{\text{eff}}$ , considering only  $H_{\pi,\text{soc}}^{\text{eff}}$ <sup>32,36</sup> as the additional term to  $H_{\pi,0}^{\text{eff}}$  is not sufficient to give the correct energy band structure, especially for the metallic nanotubes. In fact, the term  $H_{\pi,\text{cv}}^{\text{eff}}$  gives an additional spin-independent shift of the energy crossing point in two-dimensional  $k$ -space. As a consequence, the small energy gap opens for the chiral and zigzag metallic nanotubes.<sup>3,4,30,41</sup> As shown in eq. (5.8),  $H_{\pi,\text{cv}}^{\text{eff}}$  also lifts the degeneracy of the energy subband together with the term  $H_{\pi,\text{soc}}^{\text{eff}}$  for the lowest subband ( $\mu' = 0$ ) of metallic ( $\nu = 0$ ) nanotubes. These terms give the microscopic explanation for the energy splitting of metallic nanotubes, in addition to the group theoretical explanation, lack of an inversion center for the chiral nanotubes.<sup>35</sup>

As shown in eq. (5.2), not only the off-diagonal term<sup>30,32,36</sup> but also the diagonal term appear in  $H_{\pi,\text{soc}}^{\text{eff}}$ . The diagonal term of  $H_{\text{soc}}^{\text{eff}}$ , an effective Zeeman term (with opposite effective magnetic field between  $K$  and  $K'$  points), appears by considering the intermediate states of  $\sigma$  bands as the linear combination of A and B sub-lattice Bloch functions. The diagonal term together with the off-diagonal term cause the asymmetric energy band splitting between conduction and valence bands. The asymmetry becomes larger as the effective Zeeman term becomes larger with decreasing the chiral angle. The asymmetry in the recent experiment<sup>34</sup> would be explained by the present model as shown below.

Let us compare the present results with the recent experimental results.<sup>34</sup> For single-electron and single-hole regions, each corresponds to the bottom of conduction and the top of valence bands, respectively, the spin-orbit energy splitting has been reported in the transport measurement.<sup>34</sup> However the large asymmetry of the splitting,  $0.37 \pm$

0.02 meV for single-electron and  $0.21 \pm 0.01$  meV for single-hole, is observed<sup>34)</sup> which is explained by the present paper. On the other hand, the previous theories couldn't explain the asymmetry.<sup>30,32,36)</sup> The origin of the asymmetry is an additional term of the effective Zeeman term [diagonal term in eq. (5.2)] to the previous theories.<sup>30,32,36)</sup> Because the effective Zeeman term has the chiral angle dependence, the energy splitting has the chirality dependence as shown in eq. (4.1). This implies that we can evaluate the chiral angle of nanotubes from the observed energy splitting. By comparison with the numerical data and experiment,<sup>34)</sup> the nanotube for the measurement would be a type-II semi-conducting nanotube because of the larger splitting for single-electron level. Then, by fitting the experimental data with the analytic expression of eqs. (4.1) and (4.2) with the coefficients in Table I, we get the chiral angle  $\theta = 26^\circ \pm 1^\circ$  for the nanotube in the experiment. We also get the diameter in the experiment to be  $d_t = 2.0 \pm 0.1$  nm, by assuming the coupling constant  $V_{so} = 6$  meV. The possible  $(n, m)$  values are (16, 12) which has  $d_t = 1.90$  nm,  $\theta = 25.3^\circ$ , and (17, 13) which has  $d_t = 2.04$  nm,  $\theta = 25.6^\circ$ . However, the diameter in the experiment is estimated to be 5 nm.<sup>34)</sup> One possible reason of the difference between theory and experiment would be due to the spin-orbit coupling constant. The estimated diameter in the present theory is proportional to the coupling constant. Therefore the coupling constant for the nanotubes might be  $V_{so} \simeq 15$  meV, which is 2.5 times larger than that for an isolated carbon atom. If we adjust  $d_t$  to the experiments, which will need the further study.

To understand the spin-orbit interaction is also a key for application to spintronics device. The additional term, the diagonal term of eq. (5.2), would give a chirality dependence on not only the energy band structure, but also on time evolution<sup>47,48)</sup> and relaxation mechanism<sup>36)</sup> of the electron spin in carbon nanotubes. Other types of spin-orbit interaction, e.g. Rashba type interaction under gate voltage<sup>32,36,48)</sup> might also contribute to the electronic structures. Further experiments for many types of nanotubes are desired to be clear the spin-orbit interaction in nanotubes.

## 7. Conclusion

In this paper, we calculated the low energy band structures for single wall carbon nanotubes with spin-orbit interaction. The symmetry adapted Bloch function was introduced to utilize the screw symmetry of nanotubes. The non-orthogonal tight binding calculation has been done numerically for more than 300 nanotubes within the diameter between 0.7 to 2.5 nm. It has been shown that the spin-orbit interaction opens the energy gap for armchair nanotubes. The energy band splitting, which is chirality dependent, has been seen for chiral and zigzag nanotubes, while armchair nanotube does not show any splitting for the lowest conduction and highest valence band. The spin polarization direction for each splitting band is almost polarized to the nanotube axis. Especially the splitting is generally asymmetry between valence and conduction bands. The asymmetry, chirality and diameter dependences of the splitting have been explained by the effective Hamiltonian with the diagonal effective Zeeman term. By comparing with the present theory, the chiral angle of the nanotube used in the experiment<sup>34)</sup> has been estimated.

## Acknowledgment

The authors would like to thank to Dr. K. Imura for useful discussion. K.S. is supported by JSPS Research Fellowship for Young Scientists (20-4594). R.S. acknowledges Grants-in-Aid (Nos. 16076201 and 20241023) from the Ministry of Education, Culture, Sports, Science and Technology.

## Appendix: Effective Hamiltonian for $\pi$ Electrons

In this appendix, we derive the effective Hamiltonian given in eqs. (5.1)–(5.3). We use a simpler tight-binding model for this purpose, in which only the nearest neighbor hopping integral is considered, and the overlap integral between the other sites is neglected. Four atomic orbitals on each site are considered,  $2s$  and  $2p_x, 2p_y, 2p_z$  orbitals in the direction of  $x, y, z$ -axes, respectively. The  $xyz$ -coordinates are the surface coordinates defined at each atomic site (see Fig. 1). The unperturbed  $\pi$  electrons, which has two energy bands crossed at the  $K$  and  $K'$  points, are constructed from the  $p_x$  orbitals. To derive the effective Hamiltonian, the spin function defined in the  $XYZ$ -coordinate system in eq. (2.8) is adopted as the basis sets of Hamiltonian matrix. The effective Hamiltonian derived by the basis sets of eq. (2.10) is also given for comparison.

The effective Hamiltonian is written as the sum of the three terms,  $H_\pi^{\text{eff}} = H_{\pi,0}^{\text{eff}} + H_{\pi,\text{soc}}^{\text{eff}} + H_{\pi,\text{cv}}^{\text{eff}}$ . The first term,  $H_{\pi,0}^{\text{eff}}$ , will be derived by expanding the tight-binding Hamiltonian for unperturbed  $\pi$  electrons around  $K$  ( $K'$ ) point. The second and third terms,  $H_{\pi,\text{soc}}^{\text{eff}}$  and  $H_{\pi,\text{cv}}^{\text{eff}}$ , will be derived by the second order perturbation processes of the  $\sigma$ - $\pi$  hybridizations at  $K$  ( $K'$ ) point. There are two types of  $\sigma$ - $\pi$  hybridization, one is the curvature induced hybridization, and the other is the spin-orbit interaction, whose Hamiltonians are written as  $H_{\text{cv}}$  and  $H_{\text{so}}$ , respectively. Then the effective Hamiltonian, which takes into account these hybridizations, is derived as,

$$\begin{aligned} & \langle x\sigma_2 s_2 \tau_2 | H_{(\sigma-\pi)}^{\text{eff}} | x\sigma_1 s_1 \tau_1 \rangle \\ &= \sum_m \frac{\langle x\sigma_2 s_2 \tau_2 | H' | m \rangle \langle m | H' | x\sigma_1 s_1 \tau_1 \rangle}{-E_m}, \quad (\text{A.1}) \end{aligned}$$

where  $H' = H_{\text{so}} + H_{\text{cv}}$ , the summation  $m$  takes over all possible intermediate states of  $\sigma$  bands. Here the Fermi energy is taken to be zero. The initial and final states,  $|x\sigma s \tau\rangle$ , are the  $2p_x$  tight-binding function at  $K$  ( $K'$ ) point.  $\tau = 1$  ( $-1$ ) is used as the index of  $K$  ( $K'$ ) point. (In the present model we don't consider the mixing between  $K$  and  $K'$ , therefore we only have diagonal terms for  $\tau$  states.) The effective Hamiltonian  $H_{(\sigma-\pi)}^{\text{eff}}$  contains  $H_{\pi,\text{soc}}^{\text{eff}}$  in which both  $H_{\text{so}}$  and  $H_{\text{cv}}$  contribute as first order, and  $H_{\pi,\text{cv}}^{\text{eff}}$  in which  $H_{\text{cv}}$  contributes as second order. The other contributions, second order of  $H_{\text{so}}$ , and both first order of  $H_{\text{so}}$  and  $H_{\text{cv}}$  for inter-subband process, are also contained in  $H_{(\sigma-\pi)}^{\text{eff}}$ . In the following we will show the matrix elements of eq. (A.1).

### A.1 Curvature induced hybridization

First we derive the matrix elements of the curvature induced hybridization. For larger diameter nanotubes, a  $p_x$  orbital has the hopping integral between only  $p_x$  orbitals on the neighbor atoms. However when the diameter becomes smaller, the hopping between the other orbitals occurs for the finite curvature on the cylindrical surface. Since the

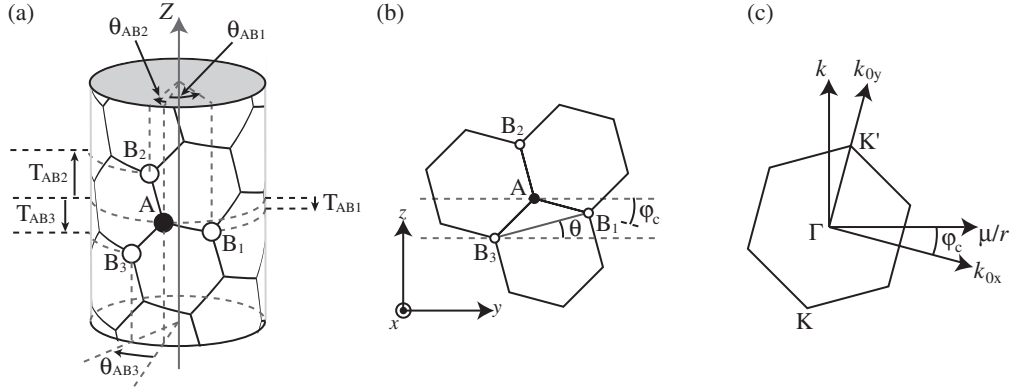


Fig. A-1. (a) Axis and circumference components of A to its neighbor three B atoms, ( $T_{ABi}, \theta_{ABi}$ ). (b) Angle between circumference direction and  $AB_1$ ,  $\varphi_c$ , and chiral angle,  $\theta$ . (c) Wave vector for nanotube, ( $k_c, k_t$ ), and that for graphene, ( $k_{0x}, k_{0y}$ ).

curvature induced hybridization itself is spin independent effect, we consider the spinless tight-binding function eq. (2.2). Extension to spin problem is simply given by adding the spin index.

First let us consider the hopping integral between  $2p_x$  orbital on a carbon A atom and  $j$  orbitals ( $j = 2s, x, y, z$ ) on its three nearest neighbor B atoms. Using the Slater-Koster type projection for the orbitals, the hopping integral between  $j$  orbital on A atom at position  $l$  and  $j'$  orbital on B atom at position  $l'$ , for both  $j, j' = x, y, z$ , is written as,<sup>30)</sup>

$$\begin{aligned} \langle \phi_{jAl} | H_0 | \phi_{j'B_l'} \rangle \\ = \mathbf{n}_{jl} \cdot \mathbf{n}_{j'l'} H_\pi - \frac{(\mathbf{L}_{l'l} \cdot \mathbf{n}_{jl})(\mathbf{L}_{l'l} \cdot \mathbf{n}_{j'l'})}{\mathbf{L}_{l'l} \cdot \mathbf{L}_{l'l}} (H_\sigma + H_\pi), \end{aligned} \quad (\text{A-2})$$

where  $\mathbf{n}_{jl}$  is the unit vector of the direction  $j$  at  $l$ , and  $\mathbf{L}_{l'l}$  is the vector from  $l$  to  $l'$ .  $H_\sigma$  is the hopping integral between  $\sigma$  orbitals, and  $H_\pi$  is that between  $\pi$  orbitals.<sup>42)</sup> Similarly, the hopping integral between  $j = x, y, z$  orbitals on A atom and  $2s$  on B atom is written as,

$$\langle \phi_{jAl} | H_0 | \phi_{2sB_l'} \rangle = \frac{\mathbf{L}_{l'l} \cdot \mathbf{n}_{jl}}{|\mathbf{L}_{l'l}|} H_{sp}, \quad (\text{A-3})$$

where  $H_{sp}$  is the hopping integral between  $2s$  and  $\sigma$  orbitals.<sup>42)</sup>

Let an A atom be on  $(r, 0, 0)$  with label  $l = 0$ , and its neighbor three B atoms be labeled by  $l = 1, 2, 3$  [see Fig. A-1(a)]. For the nanotube with chiral angle  $\theta$ , the vectors are written as,  $\mathbf{L}_{l0} = (r(\cos \theta_{AB_l} - 1), r \sin \theta_{AB_l}, T_{AB_l})$ ,  $\mathbf{n}_{xl} = (\cos \theta_{AB_l}, \sin \theta_{AB_l}, 0)$ ,  $\mathbf{n}_{yl} = (-\sin \theta_{AB_l}, \cos \theta_{AB_l}, 0)$ ,  $\mathbf{n}_{zl} = (0, 0, 1)$ , here  $T_{AB_l} = -\gamma_l(a/\sqrt{3}) \sin(\varphi_c + \delta_l)$  and  $\theta_{AB_l} = \gamma_l(a/\sqrt{3}r) \cos(\varphi_c + \delta_l)$  are the axis and angle components of the B atom on site  $l$ , where  $\gamma_l = 1, -1, -1$  and  $\delta_l = 0, \pi/3, -\pi/3$ , for  $l = 1, 2, 3$ , respectively [see Fig. A-1(a)].  $a = 2.46 \text{ \AA}$  is the lattice constant of graphene,  $\varphi_c = \pi/6 - \theta$  is the angle between circumference vector and  $\mathbf{L}_{l0}$  [see Fig. A-1(b)]. Then the hopping integrals between atomic orbitals are calculated as,

$$\langle \phi_{xA0} | H_0 | \phi_{2sB_l} \rangle = \langle \phi_{2sA0} | H_0 | \phi_{xB_l} \rangle = -\frac{1}{2\sqrt{3}} \frac{a}{r} \cos^2(\varphi_c + \delta_l) H_{sp}, \quad (\text{A-4})$$

$$\begin{aligned} \langle \phi_{xA0} | H_0 | \phi_{yB_l} \rangle &= -\langle \phi_{yA0} | H_0 | \phi_{xB_l} \rangle \\ &= -\gamma_l \frac{1}{\sqrt{3}} \frac{a}{r} \cos(\varphi_c + \delta_l) \left[ H_\pi - \frac{1}{2} (H_\pi + H_\sigma) \cos^2(\varphi_c + \delta_l) \right], \end{aligned} \quad (\text{A-5})$$

$$\begin{aligned} \langle \phi_{xA0} | H_0 | \phi_{zB_l} \rangle &= -\langle \phi_{zA0} | H_0 | \phi_{xB_l} \rangle \\ &= -\frac{1}{2\sqrt{3}} \frac{a}{r} \gamma_l \sin(\varphi_c + \delta_l) \cos^2(\varphi_c + \delta_l) (H_\pi + H_\sigma), \end{aligned} \quad (\text{A-6})$$

$$\langle \phi_{xA0} | H_0 | \phi_{xB_l} \rangle = H_\pi - \frac{1}{6} \left( \frac{a}{r} \right)^2 \cos^2(\varphi_c + \delta_l) \left[ H_\pi - \frac{1}{2} (H_\pi + H_\sigma) \cos^2(\varphi_c + \delta_l) \right]. \quad (\text{A-7})$$

Here we considered the lowest order contribution of curvature ( $a/r$ ) in each integral.

Using the above integrals, the hopping integral matrix elements between the tight-binding functions eq. (2.2) are obtained as,

$$\begin{aligned} \langle xA\mathbf{k}_0 | H_0 | 2sB\mathbf{k}_0 \rangle &= \langle 2sA\mathbf{k}_0 | H_0 | xB\mathbf{k}_0 \rangle \\ &= -\frac{1}{4\sqrt{3}} \frac{a}{r} H_{sp} [f(\mathbf{k}_0) - g(\mathbf{k}_0) \cos 2\varphi_c - h(\mathbf{k}_0) \sin 2\varphi_c], \end{aligned} \quad (\text{A-8})$$

$$\begin{aligned} \langle xA\mathbf{k}_0 | H_0 | yB\mathbf{k}_0 \rangle &= -\langle yA\mathbf{k}_0 | H_0 | xB\mathbf{k}_0 \rangle \\ &= \frac{1}{8\sqrt{3}} \frac{a}{r} [(H_\pi + H_\sigma) f(\mathbf{k}_0) \cos 3\varphi_c + (5H_\pi - 3H_\sigma)(g(\mathbf{k}_0) \cos \varphi_c - h(\mathbf{k}_0) \sin \varphi_c)], \end{aligned} \quad (\text{A-9})$$

$$\begin{aligned} \langle xA\mathbf{k}_0|H_0|zB\mathbf{k}_0\rangle &= -\langle zA\mathbf{k}_0|H|xB\mathbf{k}_0\rangle \\ &= \frac{1}{8\sqrt{3}} \frac{a}{r} (H_\sigma + H_\pi) [-f(\mathbf{k}_0) \sin 3\varphi_c + g(\mathbf{k}_0) \sin \varphi_c + h(\mathbf{k}_0) \cos \varphi_c], \end{aligned} \quad (\text{A}\cdot 10)$$

$$\begin{aligned} \langle xA\mathbf{k}_0|H_0|xB\mathbf{k}_0\rangle &= H_\pi f(\mathbf{k}_0) - \frac{1}{96} \left(\frac{a}{r}\right)^2 [f(\mathbf{k}_0)(5H_\pi - 3H_\sigma) - 4(H_\pi - H_\sigma)(g(\mathbf{k}_0) \cos 2\varphi_c + h(\mathbf{k}_0) \sin 2\varphi_c) \\ &\quad + (H_\pi + H_\sigma)(g(\mathbf{k}_0) \cos 4\varphi_c - h(\mathbf{k}_0) \sin 4\varphi_c)], \end{aligned} \quad (\text{A}\cdot 11)$$

where

$$f(\mathbf{k}_0) = \exp\left(i \frac{k_{0x}a}{\sqrt{3}}\right) + 2 \exp\left(-i \frac{k_{0x}a}{2\sqrt{3}}\right) \cos\left(\frac{k_{0y}a}{2}\right), \quad (\text{A}\cdot 12)$$

$$g(\mathbf{k}_0) = -\exp\left(i \frac{k_{0x}a}{\sqrt{3}}\right) + \exp\left(-i \frac{k_{0x}a}{2\sqrt{3}}\right) \cos\left(\frac{k_{0y}a}{2}\right), \quad (\text{A}\cdot 13)$$

$$h(\mathbf{k}_0) = \sqrt{3}i \exp\left(-i \frac{k_{0x}a}{2\sqrt{3}}\right) \sin\left(\frac{k_{0y}a}{2}\right). \quad (\text{A}\cdot 14)$$

Here we introduced the two dimensional wave vector  $\mathbf{k}_0 = (k_{0x}, k_{0y})$ , which has the following relations between  $\mathbf{k} = (k, \mu)$  as [see Fig. A·1(c)],

$$\begin{pmatrix} k_{0x} \\ k_{0y} \end{pmatrix} = \begin{pmatrix} \cos \varphi_c & -\sin \varphi_c \\ \sin \varphi_c & \cos \varphi_c \end{pmatrix} \begin{pmatrix} \mu/r \\ k \end{pmatrix}. \quad (\text{A}\cdot 15)$$

At  $K$  ( $K'$ ) point,  $\mathbf{k}_0 = 2\pi/a(0, -2/3)$  [ $\mathbf{k}_0 = 2\pi/a(0, 2/3)$ ] in this calculation, the matrix elements of eqs. (A·8)–(A·11) are simply written as,

$$\langle 2s\sigma'\tau|H_0|x\sigma\tau\rangle = -\frac{\sqrt{3}}{8} \frac{a}{r} H_{\text{sp}} e^{-2i\sigma\tau\varphi_c} \delta_{\sigma, -\sigma'}, \quad (\text{A}\cdot 16)$$

$$\langle y\sigma'\tau|H_0|x\sigma\tau\rangle = -\sigma \frac{\sqrt{3}}{16} \frac{a}{r} (5H_\pi - 3H_\sigma) e^{i\sigma\tau\varphi_c} \delta_{\sigma, -\sigma'}, \quad (\text{A}\cdot 17)$$

$$\langle z\sigma'\tau|H_0|x\sigma\tau\rangle = i\tau \frac{\sqrt{3}}{16} \frac{a}{r} (H_\pi + H_\sigma) e^{i\sigma\tau\varphi_c} \delta_{\sigma, -\sigma'}, \quad (\text{A}\cdot 18)$$

$$\langle x\sigma'\tau|H_0|x\sigma\tau\rangle = -\frac{1}{64} \left(\frac{a}{r}\right)^2 [4(H_\pi - H_\sigma) e^{-2i\sigma\tau\varphi_c} - (H_\pi + H_\sigma) e^{4i\sigma\tau\varphi_c}] \delta_{\sigma, -\sigma'}, \quad (\text{A}\cdot 19)$$

where  $\sigma = 1$  ( $-1$ ) is the index for A (B) atom. Hereafter we write the Hamiltonian of eqs. (A·16)–(A·19) as  $H_{\text{cv}}$ .

## A.2 Spin-orbit interaction

Next let us consider the matrix elements of the spin-orbit interaction. The inner product of the spin-orbit interaction in eq. (2.7) is expanded as,

$$\boldsymbol{\ell}_l \cdot \mathbf{s} = \ell_{l,+} s_- + \ell_{l,-} s_+ + \ell_{l,z} s_z, \quad (\text{A}\cdot 20)$$

where  $\ell_{l,\pm} = \ell_{l,x} \pm i\ell_{l,y}$  [ $s_{\pm} = (s_x \pm is_y)/2$ ] are the ascent/descent operators for the angular momentum (Pauli matrix for spin). The components of these operators are defined in the  $xyz$ -coordinate system at  $l$ -th atomic site. The atomic 2p-orbitals are written as the linear combinations of  $\ell_z$  eigenfunctions,

$$|\phi_{x\sigma l}\rangle = \frac{1}{\sqrt{2}} [-(\ell_z = 1)_{\sigma l} + |(\ell_z = -1)_{\sigma l}\rangle], \quad (\text{A}\cdot 21)$$

$$|\phi_{y\sigma l}\rangle = \frac{i}{\sqrt{2}} [(\ell_z = 1)_{\sigma l} + |(\ell_z = -1)_{\sigma l}\rangle], \quad (\text{A}\cdot 22)$$

$$|\phi_{z\sigma l}\rangle = |(\ell_z = 0)_{\sigma l}\rangle, \quad (\text{A}\cdot 23)$$

therefore, using the relation eq. (2.9),  $p_x$ -orbital at site  $l$  with spin  $s$  has the finite matrix elements between the orbitals as follows,

$$\langle s| \langle \phi_{y\sigma l} | H_{\text{so}} | \phi_{x\sigma l} \rangle | s \rangle = \frac{i}{2} s V_{\text{so}}, \quad (\text{A}\cdot 24)$$

$$\langle -s | \langle \phi_{z\sigma l} | H_{\text{so}} | \phi_{x\sigma l} \rangle | s \rangle = \frac{1}{2} e^{i\theta_s} s V_{\text{so}}. \quad (\text{A}\cdot 25)$$

Here the azimuth-angle dependent factor  $e^{i\theta_s}$  in eq. (A·25) appears, because the coordinate system for spin function  $|s\rangle$  is rotated from the coordinate system for atomic orbital by  $-\theta_l$ . The corresponding matrix elements between the tight-binding functions given in eq. (2.8) are given by,

$$\langle y\sigma s' \mathbf{k}' | H_{\text{so}} | x\sigma s \mathbf{k} \rangle = \frac{i}{2} s V_{\text{so}} \delta_{\mathbf{k}, \mathbf{k}'} \delta_{s, s'}, \quad (\text{A}\cdot 26)$$

$$\langle z\sigma s' \mathbf{k}' | H_{\text{so}} | x\sigma s \mathbf{k} \rangle = \frac{1}{2} s V_{\text{so}} \delta_{\mathbf{k}, \mathbf{k}'} \delta_{\mu', \mu+s} \delta_{s, -s'}. \quad (\text{A}\cdot 27)$$

As shown in eq. (A·27), the spin state  $s$  ( $= \pm 1$ ) with circumference momentum  $\mu$  has the finite matrix element between the opposite spin state  $-s$  with circumference momentum  $\mu + s$ .

## A.3 Unperturbed $\sigma$ band at $K/K'$ points

To obtain the second order perturbation processes of  $H' = H_{\text{so}} + H_{\text{cv}}$  to  $\pi$  electrons, energies and eigenfunctions of the intermediate states  $|m\rangle$  in eq. (A·1), that are the unperturbed  $\sigma$  bands at  $K$  ( $K'$ ) point, are needed. Because the unperturbed  $\sigma$  bands are spin degen-

erate, we consider the spinless states for this subsection. The Hamiltonian matrix elements between the Bloch functions eq. (2.2) for  $\sigma$  bands is obtained<sup>42)</sup> as the similar manner in subsection A.1 of this Appendix. Then, at  $K$  ( $K'$ ) the matrix can be separated into three block matrices as,

$$\begin{pmatrix} H_{01}^{(1)} & 0 & 0 \\ 0 & H_{01}^{(-1)} & 0 \\ 0 & 0 & H_{11} \end{pmatrix}, \quad (\text{A}\cdot 28)$$

where

$$H_{01}^{(\sigma)} = \begin{pmatrix} |2s, -\sigma, \tau\rangle & |(\ell_x = -\sigma\tau)\sigma\tau\rangle \\ \epsilon_{2s} & \frac{3}{\sqrt{2}}\tau e^{i\sigma\tau\varphi_c} H_{\text{sp}} \\ \frac{3}{\sqrt{2}}\tau e^{-i\sigma\tau\varphi_c} H_{\text{sp}} & 0 \end{pmatrix}, \quad (\text{A}\cdot 29)$$

and

$$H_{11} = \begin{pmatrix} |(\ell_x = \tau)A\tau\rangle & |(\ell_x = -\tau)B\tau\rangle \\ 0 & \frac{3}{2}e^{-2i\tau\varphi_c}(H_\pi + H_\sigma) \\ \frac{3}{2}e^{2i\tau\varphi_c}(H_\pi + H_\sigma) & 0 \end{pmatrix}. \quad (\text{A}\cdot 30)$$

Here  $\epsilon_{2s}$  is the energy of 2s orbital. The origin of energy is taken at energy of 2p orbital. The states indicated on the columns of each matrix denote the basis states of the matrix. The state labeled by  $\ell_x$  is defined as,

$$|(\ell_x = \pm 1)\sigma\tau\rangle = \mp \frac{1}{\sqrt{2}}(|y\sigma\tau\rangle \pm i|z\sigma\tau\rangle), \quad (\text{A}\cdot 31)$$

where the double-signs correspond to one another.

The eigenvalues and corresponding eigenfunctions of  $H_{01}^{(\sigma)}$  are,

$$E_{01,\eta} = \frac{1}{2} \left( \epsilon_{2s} + \eta \sqrt{\epsilon_{2s}^2 + 18H_{\text{sp}}^2} \right), \quad (\text{A}\cdot 32)$$

$$|m_{01}; \eta\sigma\tau\rangle = -\eta\tau c_\eta |2s, -\sigma, \tau\rangle + c_{-\eta} e^{-i\sigma\tau\varphi_c} |(\ell_x = -\sigma\tau)\sigma\tau\rangle, \quad (\text{A}\cdot 33)$$

and, these for  $H_{11}$  are,

$$E_{11,\eta} = \frac{3}{2} \eta (H_\pi + H_\sigma), \quad (\text{A}\cdot 34)$$

$$|m_{11}; \eta\tau\rangle = \frac{1}{\sqrt{2}} \sum_{\sigma} (-1)^{\frac{1-\eta}{2}\frac{1-\sigma}{2}} e^{i\sigma\tau\varphi_c} |(\ell_x = \sigma\tau)\sigma\tau\rangle. \quad (\text{A}\cdot 35)$$

Here  $\eta = \pm 1$  indicates the two eigenstates for each block matrix, and,  $c_\eta$  is given by,

$$c_\eta = \sqrt{\frac{\eta E_{01,\eta}}{E_{01,+} - E_{01,-}}}. \quad (\text{A}\cdot 36)$$

#### A.4 Effective Hamiltonian

Using the results of eqs. (A.16)–(A.19), (A.31), (A.33) and (A.35) with adding the spin degree of freedom, and eqs. (A.26) and (A.27), the matrix elements between  $\pi$  states,  $|\chi\sigma\tau\rangle$ , and intermediate  $\sigma$  states,  $|m_{01}; \eta\sigma\tau\rangle$  and  $|m_{11}; \eta\tau\rangle$ , are written for the curvature induced hybridization as,

$$\langle m_{01}; \eta\sigma' s' \tau' | H_{\text{cv}} | \chi\sigma\tau \rangle = \frac{\sqrt{3}}{8} \frac{a}{r} [\sqrt{2} c_{-\eta} (H_\pi - H_\sigma) \delta_{\sigma, -\sigma'} + \eta c_\eta e^{-2i\sigma\tau\varphi_c} H_{\text{sp}} \delta_{\sigma, \sigma'}] \tau \delta_{s, s'} \delta_{\tau, \tau'}, \quad (\text{A}\cdot 37)$$

$$\langle m_{11}; \eta s' \tau' | H_{\text{cv}} | \chi\sigma\tau \rangle = \frac{\sqrt{3}}{16} \frac{a}{r} (-1)^{\frac{1-\eta}{2}\frac{1+\sigma}{2}+1} e^{2i\sigma\tau\varphi_c} (3H_\pi - H_\sigma) \tau \delta_{s, s'} \delta_{\tau, \tau'}, \quad (\text{A}\cdot 38)$$

and for the spin-orbit interaction as,

$$\langle m_{01}; \eta\sigma' s' \tau' | H_{\text{so}} | \chi\sigma\tau \rangle = \frac{i c_{-\eta}}{2\sqrt{2}} e^{i\sigma\tau\varphi_c} s (\sigma\tau \delta_{s, s'} + \delta_{s, -s'} \delta_{\mu, \mu' - s}) \delta_{\sigma, \sigma'} \delta_{\tau, \tau'}, \quad (\text{A}\cdot 39)$$

$$\langle m_{11}; \eta s' \tau' | H_{\text{so}} | \chi\sigma\tau \rangle = \frac{i}{4} (-1)^{\frac{1-\eta}{2}\frac{1-\sigma}{2}} e^{-i\sigma\tau\varphi_c} s (-\sigma\tau \delta_{s, s'} + \delta_{s, -s'} \delta_{\mu, \mu' - s}) \delta_{\tau, \tau'}, \quad (\text{A}\cdot 40)$$

where the second terms in eqs. (A.39) and (A.40) denote the inter-subband mixing with spin flipping. The index  $\mu$  ( $\mu'$ ) belongs to the index  $\tau$  ( $\tau'$ ). The other terms in eqs. (A.37)–(A.40) denote the intra-subband processes, and we omit  $\delta_{\mu, \mu'}$  in these expressions.

Now we derive the effective Hamiltonian. Using eqs. (A.32), (A.34), and (A.37)–(A.40) for the second order perturbation expansion in the right hand side of eq. (A.1), we get the following effective Hamiltonian,

$$\begin{aligned} \tilde{H}_{\pi, \text{soc}}^{\text{eff}} &= [A_1 (\cos \varphi_c \hat{\sigma}_y \hat{\tau}_I - \sin \varphi_c \hat{\sigma}_x \hat{\tau}_z) \\ &\quad + A_2 \sin 3\varphi_c \hat{\sigma}_I \hat{\tau}_z] \hat{s}_Z, \end{aligned} \quad (\text{A}\cdot 41)$$

$$\begin{aligned} \tilde{H}_{\pi, \text{cv}}^{\text{eff}} &= [(B_1 \cos 2\varphi_c + B_2 \cos 4\varphi_c) \hat{\sigma}_x \hat{\tau}_I \\ &\quad + (-B_1 \sin 2\varphi_c + B_2 \sin 4\varphi_c) \hat{\sigma}_y \hat{\tau}_z] \hat{s}_I, \end{aligned} \quad (\text{A}\cdot 42)$$

for intra-subband processes. Here  $\hat{\sigma}$ ,  $\hat{s}$ ,  $\hat{\tau}$  are the Pauli matrix operators for the states  $|\sigma\rangle$ ,  $|s\rangle$ ,  $|\tau\rangle$ , respectively. The suffix  $I$  denotes the unit matrix. The coefficients are written as,

$$A_1 = \frac{(H_\pi - H_\sigma) \epsilon_{2s}}{12\sqrt{3}H_{\text{sp}}^2} V_{\text{so}} \frac{a}{r}, \quad (\text{A}\cdot 43)$$

$$A_2 = -\frac{H_\pi}{2\sqrt{3}(H_\pi + H_\sigma)} V_{\text{so}} \frac{a}{r}, \quad (\text{A}\cdot 44)$$

$$B_1 = -\frac{H_\pi - H_\sigma}{32} \left(\frac{a}{r}\right)^2, \quad (\text{A}\cdot 45)$$

$$B_2 = -\frac{H_\pi(H_\pi - H_\sigma)}{8(H_\pi + H_\sigma)} \left(\frac{a}{r}\right)^2. \quad (\text{A}\cdot 46)$$

The term (A.41) is proportional to both the spin-orbit interaction and the curvature of nanotube,  $V_{\text{so}}(a/r)$ , and the term (A.42) is proportional to the square of curvature,  $(a/r)^2$ . To derive the term (A.42), we also added the contribution from eq. (A.19).

By expanding the first term of eq. (A.11) around  $K$  and  $K'$  points, we get the unperturbed effective Hamiltonian for  $\pi$  electrons as

$$\tilde{H}_{\pi,0}^{\text{eff}} = \hbar v_F \begin{pmatrix} 0 & -ie^{-i\tau\varphi_c}(k_c - i\tau k_l) \\ ie^{i\tau\varphi_c}(k_c + i\tau k_l) & 0 \end{pmatrix}, \quad (\text{A}\cdot 47)$$

The Fermi velocity can be written by the hopping parameter as,  $v_F = -\sqrt{3}aH_\pi/2\hbar$ . By performing the unitary transformation,  $H_{\pi,0}^{\text{eff}} = U\tilde{H}_{\pi,0}^{\text{eff}}U^{-1}$ , with the following unitary matrix,

$$U = \begin{pmatrix} ie^{i\tau\varphi_c} & 0 \\ 0 & 1 \end{pmatrix}, \quad (\text{A}\cdot 48)$$

we get the unperturbed Hamiltonian shown in eq. (5.1). Both the terms (A-41) and (A-42) have the diagonal form for  $\hat{s}_Z$  and  $\hat{\tau}_z$ , therefore these can be written as the matrix form of  $\hat{\sigma}_z$ . After the same unitary transformation with eq. (A-48), we get the effective Hamiltonian as shown in eqs. (5.2) and (5.3).

Equation (A-41) is divided into two terms, off-diagonal term proportional to  $A_1$  and diagonal term proportional to  $A_2$ . The off-diagonal term has also been pointed out in the previous calculations,<sup>30,32,36</sup> and affects as the spin-dependent shift of the energy crossing point in two dimensional  $k$ -space. On the other hand, the diagonal term in eq. (5.2) is obtained in this calculation. The diagonal term appears by considering the intermediate states of  $\sigma$  bands as the linear combination of A and B sub-lattice Bloch functions, as shown in eqs. (A-33) and (A-35). The diagonal term affects as an effective Zeeman term with the opposite effective magnetic field between  $K$  and  $K'$  points.

The parameters in eqs. (5.4)–(5.7) are given by,

$$\alpha_1 = -\frac{a(H_\pi - H_\sigma)\epsilon_{2s}}{6\sqrt{3}H_{\text{sp}}^2}, \quad (\text{A}\cdot 49)$$

$$\alpha_2 = -\frac{aH_\pi}{\sqrt{3}(H_\pi + H_\sigma)}, \quad (\text{A}\cdot 50)$$

$$\beta = -\frac{a^2(H_\pi - H_\sigma)(H_\sigma - 3H_\pi)}{8(H_\pi + H_\sigma)}, \quad (\text{A}\cdot 51)$$

$$\zeta = \frac{a(H_\pi - H_\sigma)(H_\sigma + 5H_\pi)}{4\sqrt{3}H_\pi(H_\pi + H_\sigma)}. \quad (\text{A}\cdot 52)$$

If we use the values,  $H_\pi = -3.033$  eV,  $H_\sigma = -5.037$  eV,  $H_{\text{sp}} = -5.580$  eV and  $\epsilon_{2s} = -8.868$  eV,<sup>4,42</sup> then we get  $\alpha_1 = 0.014$  nm,  $\alpha_2 = -0.054$  nm,  $\beta = 7.8$  meV·nm<sup>2</sup>,  $\zeta = -0.060$  nm. However, these parameters should be estimated by more precise calculation, e.g., the numerical calculation shown in this paper, or by experiments.

To derive (A-41), we restricted only the intra-subband processes in eqs. (A-39) and (A-40). It is important to stress that there is also inter-subband mixing with spin flipping as we discussed in eqs. (A-39) and (A-40). The corresponding effective Hamiltonian is written as,

$$\tilde{H}_{\text{soc, inter}}^{\text{eff}} = [A_1(\sin \varphi_c \hat{\sigma}_y \hat{\tau}_l + \cos \varphi_c \hat{\sigma}_x \hat{\tau}_z) - A_2 \cos 3\varphi_c \hat{\sigma}_l \hat{\tau}_z] i(-\hat{s}_+ \hat{\mu}_- + \hat{s}_- \hat{\mu}_+), \quad (\text{A}\cdot 53)$$

where  $\hat{\mu}_\pm$  are the ascent/descent operators for subband index  $\mu$ . Fortunately, the term can be safely neglected if the energy difference of two subbands is large enough compared with  $A_1$  and  $A_2$ . However the term should also be considered for spin relaxation processes in long time.<sup>30,36</sup> We also get the second order contribution of spin-orbit interaction as,

$$\tilde{H}_{\text{so}^2}^{\text{eff}} = -\frac{\epsilon_{2s}V_{\text{so}}^2}{18H_{\text{sp}}} \hat{\sigma}_z \hat{\tau}_z (\hat{s}_+ \hat{\mu}_- + \hat{s}_- \hat{\mu}_+). \quad (\text{A}\cdot 54)$$

The corresponding term also appears for the flat graphene problem.<sup>31–33,49</sup> The term can be safely neglect because the energy scale of the factor is sufficiently small,  $\epsilon_{2s}V_{\text{so}}^2/18H_{\text{sp}} \sim 1$   $\mu$ eV. Note that, when we use the symmetry adapted Bloch function, eq. (2.10), instead of eq. (2.8) for the basis state, we get the effective Hamiltonian by changing,  $(\hat{s}_+ \hat{\mu}_- + \hat{s}_- \hat{\mu}_+) \rightarrow \hat{\hat{s}}_x$ ,  $(\hat{s}_+ \hat{\mu}_- - \hat{s}_- \hat{\mu}_+)/i \rightarrow \hat{\hat{s}}_y$ ,  $\hat{s}_Z \rightarrow \hat{\hat{s}}_z$ ,  $\hat{s}_I \rightarrow \hat{\hat{s}}_I$ . The relation of eq. (2.20) should also be considered in the term (5.1) for this case, which will be reported elsewhere.

- 1) P. Avouris: *Phys. Today* **62** (2009) No. 1, 34.
- 2) J. W. Mintmire, B. I. Dunlap, and C. T. White: *Phys. Rev. Lett.* **68** (1992) 631.
- 3) N. Hamada, S. Sawada, and A. Oshiyama: *Phys. Rev. Lett.* **68** (1992) 1579.
- 4) R. Saito, M. Fujita, G. Dresselhaus, and M. S. Dresselhaus: *Phys. Rev. B* **46** (1992) 1804.
- 5) R. Saito, M. Fujita, G. Dresselhaus, and M. S. Dresselhaus: *Appl. Phys. Lett.* **60** (1992) 2204.
- 6) J. W. G. Wildöer, L. C. Venema, A. G. Rinzler, R. E. Smalley, and C. Dekker: *Nature* **391** (1998) 59.
- 7) T. W. Odom, J.-L. Huang, P. Kim, and C. M. Lieber: *Nature* **391** (1998) 62.
- 8) K. Tsukagoshi, B. W. Alphenaar, and H. Ago: *Nature* **401** (1999) 572.
- 9) B. Zhao, I. Mönch, H. Vinzelberg, T. Mühl, and C. M. Schneider: *Appl. Phys. Lett.* **80** (2002) 3144.
- 10) J.-R. Kim, H. M. So, J.-J. Kim, and J. Kim: *Phys. Rev. B* **66** (2002) 233401.
- 11) S. Sahoo, T. Kontos, C. Schönenberger, and C. Sürgers: *Appl. Phys. Lett.* **86** (2005) 112109.
- 12) A. Jensen, J. R. Hauptmann, J. Nygård, and P. E. Lindelof: *Phys. Rev. B* **72** (2005) 035419.
- 13) S. Sahoo, T. Kontos, J. Furer, C. Hoffmann, M. Gräber, A. Cottet, and C. Schönenberger: *Nat. Phys.* **1** (2005) 99.
- 14) H. T. Man, I. J. W. Wever, and A. F. Morpurgo: *Phys. Rev. B* **73** (2006) 241401.
- 15) N. Tombros, S. J. van der Molen, and B. J. van Wees: *Phys. Rev. B* **73** (2006) 233403.
- 16) L. E. Hueso, J. M. Pruneda, V. Ferrari, G. Burnell, J. P. Valdés-Herrera, B. D. Simons, P. B. Littlewood, E. Artacho, A. Fert, and N. D. Mathur: *Nature* **445** (2007) 410.
- 17) C. A. Merchant and N. Marković: *Phys. Rev. Lett.* **100** (2008) 156601.
- 18) G. Gunnarsson, J. Trbovic, and C. Schönenberger: *Phys. Rev. B* **77** (2008) 201405.
- 19) W. Liang, M. Bockrath, and H. Park: *Phys. Rev. Lett.* **88** (2002) 126801.
- 20) D. H. Cobden and J. Nygård: *Phys. Rev. Lett.* **89** (2002) 046803.
- 21) S. Moriyama, T. Fuse, M. Suzuki, Y. Aoyagi, and K. Ishibashi: *Phys. Rev. Lett.* **94** (2005) 186806.
- 22) P. Jarillo-Herrero, J. Kong, H. S. J. van der Zant, C. Dekker, L. P. Kouwenhoven, and S. D. Franceschi: *Phys. Rev. Lett.* **94** (2005) 156802.
- 23) P. Jarillo-Herrero, J. Kong, H. S. J. van der Zant, C. Dekker, L. P. Kouwenhoven, and S. D. Franceschi: *Nature* **434** (2005) 484.
- 24) S. Săpmaz, P. Jarillo-Herrero, J. Kong, C. Dekker, L. P. Kouwenhoven, and H. S. J. van der Zant: *Phys. Rev. B* **71** (2005) 153402.
- 25) J. Cao, Q. Wang, and H. Dai: *Nat. Mater.* **4** (2005) 745.
- 26) A. Makarovski, J. Liu, and G. Finkelstein: *Phys. Rev. Lett.* **99** (2007) 066801.
- 27) A. Makarovski, A. Zhukov, J. Liu, and G. Finkelstein: *Phys. Rev. B* **75** (2007) 241407.
- 28) J. V. Holm, H. I. Jørgensen, K. Grove-Rasmussen, J. Paaske, K. Flensberg, and P. E. Lindelof: *Phys. Rev. B* **77** (2008) 161406.
- 29) C. J. Rauch: *Proc. Int. Conf. Physics of Semiconductors* (Institute of Physics, London, 1962) p. 276.
- 30) T. Ando: *J. Phys. Soc. Jpn.* **69** (2000) 1757.
- 31) H. Min, J. E. Hill, N. A. Sinitsyn, B. R. Sahu, L. Kleinman, and A. H.

- MacDonald: *Phys. Rev. B* **74** (2006) 165310.
- 32) D. Huertas-Hernando, F. Guinea, and A. Brataas: *Phys. Rev. B* **74** (2006) 155426.
- 33) Y. Yao, F. Y. X.-L. Qi, S.-C. Zhang, and Z. Fang: *Phys. Rev. B* **75** (2007) 041401.
- 34) F. Kuemmeth, S. Ilani, D. C. Ralph, and P. L. McEuen: *Nature* **452** (2008) 448.
- 35) L. Chico, M. P. Lopez-Sancho, and M. C. Muñoz: *Phys. Rev. Lett.* **93** (2004) 176402.
- 36) D. V. Bulaev, B. Trauzettel, and D. Loss: *Phys. Rev. B* **77** (2008) 235301.
- 37) C. T. White, D. H. Robertson, and J. W. Mintmire: *Phys. Rev. B* **47** (1993) 5485.
- 38) V. N. Popov: *New J. Phys.* **6** (2004) 17.
- 39) G. G. Samsonidze, R. Saito, N. Kobayashi, A. Grüneis, J. Jiang, and A. Jorio: *Appl. Phys. Lett.* **85** (2004) 5703.
- 40) D. Porezag, T. Frauenheim, T. Köhler, G. Seifert, and R. Kaschner: *Phys. Rev. B* **51** (1995) 12947.
- 41) C. L. Kane and E. J. Mele: *Phys. Rev. Lett.* **78** (1997) 1932.
- 42) R. Saito, G. Dresselhaus, and M. S. Dresselhaus: *Physical Properties of Carbon Nanotubes* (Imperial College Press, London, 1998).
- 43) A similar calculation by the authors independently suggests  $V_{so} = 5.93$  meV.
- 44) R. Saito, K. Sato, Y. Oyama, J. Jiang, G. G. Samsonidze, G. Dresselhaus, and M. S. Dresselhaus: *Phys. Rev. B* **72** (2005) 153413.
- 45) T. Ando: *J. Phys. Soc. Jpn.* **74** (2005) 777.
- 46) H. Ajiki and T. Ando: *J. Phys. Soc. Jpn.* **62** (1993) 1255.
- 47) A. D. Martino, R. Egger, K. Hallberg, and C. A. Balseiro: *Phys. Rev. Lett.* **88** (2002) 206402.
- 48) A. D. Martino and R. Egger: *J. Phys.: Condens. Matter* **17** (2005) 5523.
- 49) C. L. Kane and E. J. Mele: *Phys. Rev. Lett.* **95** (2005) 226801.